A Biologically Accurate Simulation of the Locomotion of *Caenorhabditis elegans*

Roger Mailler, Jacob Graves, Nathan Willy, and Trevor Sarratt
Computational Neuroscience and Adaptive Systems Laboratory
University of Tulsa
Tulsa, United States
{*mailler, jacob-graves, nathan-willy, trevor-sarratt*}*@utulsa.edu*

***Abstract*—The nematode *Caenorhabditis elegans* is an important model organism for many areas of biological research including genetics, development, and neurobiology. It is the first organism to have its genome sequenced, complete cell ontogeny determined, and nervous system mapped. With all of the information that is available on this simple organism, *C. elegans* may also become the first organism to be accurately and completely modeled *in silico*. This work takes a first step toward this goal by presenting a biologically accurate, 3-dimensional simulated model of *C. elegans*. This model takes into account many facets of the organism including size, shape, weight distribution, muscle placement, and muscle force. It also explicitly models the environment of the worm to include factors such as contact, friction, inertia, surface tension, and gravity. The model was tuned and validated using video recordings taken of the worm to show that it accurately depicts the physics of undulatory locomotion used to forward and reverse crawl on an agar surface. The main contribution of this article is a new, highly detailed 3D physics model and supporting simulator that accurately reproduces the physics of *C. elegans* locomotion.**

***Keywords*-Simulation, Biology, *Caenorhabditis elegans*, Modeling**

I. Introduction

Nearly 50 years ago, Sydney Brenner introduced *Caenorhabditis elegans* as a model for studying developmental biology and neurology. Because of its simplicity, it has become one of the best understood organisms on the planet being the only one to have its cell lineage, genome, and nervous system completely mapped. However, despite all of the effort that has gone into uncovering the secrets behind "the mind of the worm," we still lack a compelling systems-level understanding for how the neurons and the connections between them generate the surprisingly complex range of behaviors that are observed in this relatively simple organism.

One potential approach to addressing this issue is to use computer simulations that model aspects of the worm's body and nervous system [1]. For example, numerous computer simulations have been created that replicate the locomotion of *C. elegans* [2], [3], [4], [5].

Like all models, these simulations make simplifying assumptions that make them computationally tractable at the expense of accuracy. Each of them, for instance, represents the body as a set of uniformly distributed points in two-dimensional space. This prevents them from replicating the proper weight distribution, and more importantly, the non-uniform placement of the muscles that are used to generate locomotive force in the actual worm. In addition, they also fail to directly simulate the environment, but instead apply constant frictional forces at these discrete points along the body. These simplifying assumptions limit the ability of these simulations to accurately depict the non-uniform friction that results from the worm's contact with the world around it and subsequently the complex neural control that is needed to generate the worm's characteristic sinusoidal pattern of locomotion.

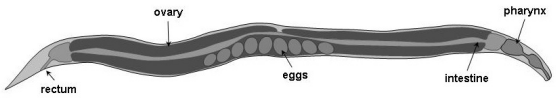

Figure 1. Basic anatomy of an adult hermaphrodite.

Leveraging the tremendous increases in computational power and advances in numeric methods, this work, which is an extended version of the work presented in [1], seeks to rectify these deficiencies by developing a biologically accurate 3D model of the body of *C. elegans* in a virtual environment that mirrors the physical properties of its natural world. This simulator, which has been under development for nearly two years, is built using an open-source 3D game and physics engine. The model accurately depicts the physical properties of the real organism including its non-uniform weight, size, shape, and musculature. In addition, the simulator models the interaction between the worm and its environment to include surface tension, friction, inertia, and gravity.

This paper presents this new model and demonstrates that it faithfully reproduces forward and reverse crawling of *C. elegans* on an agar surface. The model is cross validated using video recordings of worms that were converted to quantitative data by image analysis software. During our validation, we found that, during forward locomotion, the forces generated by the muscles may decrease as the wave propagates from the worm's head to its tail. Although we

found no mention of this in the literature, the placement of the muscles in the worm's body, along with video analysis of the worm's crawling gait seem to support our finding. We also have found that in order to replicate reverse locomotion that the force generated by the muscles needed to be higher, the wavelength shorter, and the wave propagation slower.

The rest of this article is organized as follows. In Section II, a brief introduction to the anatomy of C. elegans is given along with a review of other approaches to modeling this organism. In Section III, we present the underlying simulation technology used in this work as well as provide a detailed description of the physics model. In Section IV, the methods and techniques used to tune and validate the system are described with Section V discussing the results. Finally, in Section VI, we present our conclusions.

II. Background

This section provides the necessary background on the anatomy of *C. elegans* as well as the state-of-the-art in computer simulations of this organism.

A. Caenorhabditis elegans *Anatomy*

Caenorhabditis elegans is a small (1 millimeter in length) nematode that can be found living in the soil of many parts of the world. It lives by feeding on bacteria and is capable of reproducing in about 3 days under the right conditions. *C. elegans* can either be male or hermaphrodite, with males occurring at a low frequency in the population. They reproduce by either self fertilization in the hermaphrodite or by mating a male and hermaphrodite. Hermaphrodites lay about 300 eggs during their approximately 15 day lifespan.

C. elegans (see Figure 1) is a very simple organism, with only 959 cells in the adult hermaphrodite and 1031 in the adult male [6]. Like other members of the nematode (Nematoda) family, the body of *C. elegans* is composed of two concentric tubes separated by a pseudocoelom. The inner tube is in the intestine and the outer tube consists of the hypodermis, muscles, nerves and the gonads. The pseudocoelom is filled with a hydrostatically pressurized fluid that helps maintain the shape of its body.

C. elegans maintains an outer cuticle, which is secreted by the hypodermis. During the lifespan of the worm, it molts its cuticle four times, punctuating the four phases of its life cycle. The cuticle, containing mostly collagen, is tough although not rigid. Adult nematodes have lateral, longitudinal seam cells on the surface of their cuticle that form treads (alae). When on a solid surface, the nematode crawls on one side with a set of treads contacting the surface.

The main body wall muscles of *C. elegans* are arranged in four rows, two dorsal and two ventral. Each row consists of 23 or 24 muscle cells that are arranged in an interleaving pattern [7]. Toward the anterior of the worm, the cells occur in overlapping pairs with less overlap and pairing occurring toward the posterior. The worm moves by propagating waves either forward or backward along its body creating a sinusoidal pattern of locomotion.

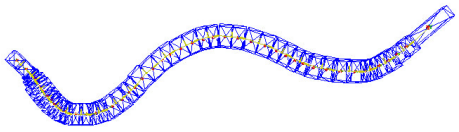

Figure 2. Physics model of the nematode *C. elegans*

C. elegans has a simple nervous system consisting of 302 neurons with about 2000 neuromuscular junctions, 5000 chemical synapses, and 700 gap junctions in the adult hermaphrodite [8]. Most of these cells are located near the pharynx and in the tail. Processes from these neurons form a "nerve ring" that surrounds the pharynx or are part of bundles that run the length of the body. The most noticeable of these bundles are the ventral and dorsal nerve cords.

The nervous system receives input primarily from sensilla located in the head of the worm that are connected to sensory neurons that extend from the nerve ring. The nerve ring sends its output through motor neuron axons that are in the ring itself or located in the ventral or dorsal nerve cords. Most neurons in *C. elegans* have simple structures with one or two processes [9]. Despite their apparent simple structure, neurons in *C. elegans* have a diverse set of voltage-gated, chemically-gated, and mechanically-gated ion channels, use many of the neurotransmitters found in vertebrates, and exhibit a complex mechanism for vesicle production, docking, priming, and release. There is considerable evidence the neurons in *C. elegans* use acetylcholine, GABA, dopamine, serotonin, glutamate, and a set of peptides in communicating with one another [8]. Acetylcholine is used as the primary excitatory neurotransmitter in motor neurons [10]. GABA is used as both an inhibitory and excitatory neurotransmitter [10]. Dopamine appears to influence egg-laying and exists in the male reproductive apparatus [11], [12]. At least ten cells in hermaphrodites seem to signal with serotonin. The strongest influence appears in the pharynx [13], although it influences egg-laying behavior as well [14]. Finally, glutamate seems to be used as both an excitatory and inhibitory neurotransmitter in motor and sensory neurons [15].

Neurons in *C. elegans* appears to contain both voltage-gated potassium and calcium channels [10], but recent advances in electro-physiological techniques have demonstrated that they seem to lack voltage-gated, sodium channels [16]. Because of this, these studies have found that neurons in the organism lack traditional, fast action potentials found in vertebrates. Instead, patch-clamping studies have been able to demonstrate non-linear, graded depolarization as a result of outward potassium flow, which is regulated by inward calcium flow [16].

Even though the nervous system of *C. elegans* has been

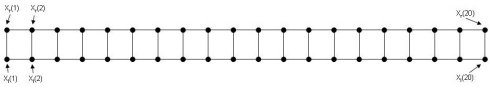

Figure 3. Uniform, two-dimensional model of *C. elegans*

physically mapped [9], the properties, roles, and interdependencies of many of the neurons are still unknown. Much of what is known about the role of individual neurons in *C. elegans* comes from behavioral studies of worms that have a genetic mutation or have undergone laser micro-dissection. As the name implies, laser micro-dissection works by killing an individual cell or group of cells using a laser [17]. Once the cells have been ablated, the behavior of the worm is observed and the role of the neuron identified. For example, using laser ablation, the role of many of the cells in pharyngeal pumping have been determined [18] and several classes of inter-neurons (AIY, AIZ, and RIB) have been found to be involved in controlling locomotion [19], [20]. In addition, the suspected roles of the D-type motor neurons have been uncovered using this technique [21]. More recent work has uncovered the importance of mechano-sensation in determining swimming gait in the worm by ablating the ALM touch receptor neuron [22].

There are a number of ways to measure the behavior of *C. elegans*. The most prominent techniques that are used include measuring changes in frequency, amplitude, or gait during locomotion [23], [3] and using chemotaxis and thermotaxis assays [24].

Even with these techniques, many questions about the function of the nervous system remain unanswered. For example, there are currently three hotly debated theories that attempt to explain how the nervous system generates and propagates waves through the worm's body given its pattern of connectivity. The first theory is that the gap junctions between muscle cells or the motor neurons aid in the propagation of the wave [9], [25]. The second theory is that *C. elegans* undulatory motion could be controlled by a central pattern generator (CPG) like the related nematode Ascaris [26], [27]. The third theory is that stretch receptors, mechanically-gated ion channels, contained within A-type and B-type motor neurons "sense" a wave and then propagate it.

B. C. elegans Simulators

All of the simulators that have, thus far, been created for *C. elegans* are designed to address specific questions about the biology of the worm that cannot be answered using standard biological techniques. The earliest use of a *C. elegans* specific simulator can be found in the work of Niebur and Erdos [2], [27]. Their simulator was designed to investigate the physical mechanics that are used to propel the organism and to determine if stretch receptor control

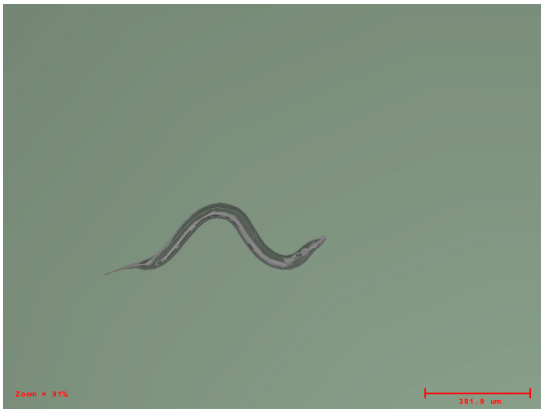

Figure 4. Screenshot of the ALIVE Simulator

could be responsible for generating the worm's characteristic sinusoidal wave.

To show that stretch receptors could create the sinusoidal wave, Niebur and Erdos created a simplified two-dimensional model of the worm that represents the contact between the worm's body and an agar surface (see Figure 3). Their model uses 40 points, 20 on the left and 20 on the right, which are evenly distributed along the length of the body. Each point is connected to the points that are contra-lateral, anterior, and posterior to it by springs that represent the cuticle of the worm. The model is powered by muscles that are connected to the points along the length of the worm. Locomotion occurs when the simulated nervous system causes the muscles to contract. The simulator then updates the position of each of the points based on the forces being created by the muscles, the elasticity of the cuticle, the interior pressure, and the frictional forces of the body's contact with the surface.

Although they did not create an accurate model of the nervous system, Niebur and Erdos were able to demonstrate that sinusoidal waves could be produced by stretch receptors located on the motor neurons that control the body wall muscles of *C. elegans*. Other researchers have extended their model in an effort to further strengthen the stretch receptor hypothesis. For example, Wakabayashi extended it by adding diagonal springs for stability and then used the resulting model to investigate several potential locomotion control methods including central pattern generator and stretch receptor control [4]. Using a fairly accurate recreation of the locomotion neural circuit, Cohen et al. have made extensive use of this model to study the use of stretch receptors for creating the phase lag of the wave [28], [5], discount the role that gap junctions play in muscle control [29], and most recently to demonstrate that the worm uses a single gait in liquids of varying viscosity [30].

Several other models have been created that explicitly model the physical body of *C. elegans*. For example, Suzuki et al., used a 12-link rigid segment model to replicate the

Table I
BODY SEGMENT SIZES (ALL NUMBERS IN μm)

i	l_i	r_i	**i**	l_i	r_i	**i**	l_i	r_i
1	50	24	**10**	45	40	**19**	35	40
2	10	28	**11**	30	40	**20**	50	40
3	15	34	**12**	55	40	**21**	55	40
4	25	40	**13**	40	40	**22**	30	40
5	20	40	**14**	50	40	**23**	40	38
6	25	40	**15**	40	40	**24**	50	32
7	20	40	**16**	50	40	**25**	100	24
8	40	40	**17**	55	40			
9	30	40	**18**	40	40			

worm's response to touch [31]. Ronkko and Wong, on the other hand, used a three-dimensional particle-based model to explore the worm's swimming and crawling behavior in various substrates including agar, water, and soil [32]. Finally Ferree, Marcotte, and Lockery built a model worm that moves forward at a constant velocity, but changes direction using a neural network that has been trained to replicate chemotaxis behavior [33], [34].

A number of simulators have also been constructed that model aspects of the nervous system without explicitly modeling the body of the worm. The work of Karbowski et al. simulates the neural circuits involved in locomotion [3]. Using a custom simulator, Wicks, Roehrig, and Rankin built a model of the neural network that controls the tap withdrawal response and by systematically analyzing it, were able to derive a possible functional relationship between some neurons in this circuit [35].

III. SIMULATOR

To develop the core of our simulation framework (see Figure III), we chose to use a Java-based high performance 3D game engine called the Java Monkey Engine (JME) [36]. Originally created by Mark Powell and now in its third major revision, JME provides all of the major features found in commercial quality game engines including loading and manipulation of 3D meshes, lighting and shadows, sound effects, animation, and terrain. JME uses a scene graph based API that allows developers to easily modify composed objects in their scene and the game engine to quickly cull branches of the graph during rendering. This makes it both easy to use and exceptionally fast.

At the core of our simulation framework is the Open Dynamics Engine (ODE) [37], which interfaces with JME using JME Physics [38]. ODE is designed to simulate articulated rigid body physics. Objects in the simulation are built from various 3D shapes that are connected to one another by joints. ODE allows users to specify the properties of the objects including weight, surface friction, and center of gravity. Joints can be created between the objects and up to six degrees of freedom are supported.

ODE uses a highly stable, first-order implicit Euler integrator. Although not quite as accurate as a fourth-order Runge-Kutta integrator, it is remarkably fast and with small enough time steps provides very realistic physical approximations. ODE handles contact and friction using a version of the Dantzig Linear Complementarity Problem (LCP) solver that was described in [39]. However, it uses a faster Coloumb friction model to optimize speed. ODE is used in a number of research and commercial robotics simulators including Gazebo [40], Marilou [41], and Webots [42].

A. Physics Model

Because ODE is designed to simulate rigid objects, we modeled the body as set of 25 discrete segments $S_i = \{1, \cdots, 25\}$ (see Figure 2). As a notational convenience we refer to segments by their index number and use the subscript i in equations to denote the segment S_i. Each segment is represented using a 3D box whose width and height are estimated by the radius, r_i, taken from photographs of living worms and length, l_i, are given by the spacing between subsequent muscle cell locations along the worm's anterior-posterior axis (see Table I). These muscle cell locations, which are taken from [43], represent the main points of powered articulation along the body .

The volume of each segment can be calculated by

$$v_i = 4r_i^2 \times l_i \tag{1}$$

and their mass, w_i, is a fraction of the total mass W and can be calculated by

$$w_i = \frac{W \times v_i}{v_{total}} \tag{2}$$

This representation creates non-uniform weights and sizes for the individual sections of the worm. This, in turn, impacts the shape and frictional properties associated with the contact surface between the worm and its environment.

Subsequent segments of the body, S_i and S_{i+1}, are connected to one another by a powered rotational joint, J_k. Like segments, we use the notational convenience of referring to the joint by its index number and use the subscript k to denote joint J_k. These joints have 2 degrees of freedom and have an angle at time t that is represented as a 3D vector $\vec{\theta}_k(t)$. The angular velocity of this joint $\vec{v}_k(t)$, is also represented as a vector with each element being the change in the corresponding angle over time.

The values of $\vec{\theta}_k(t)$ and $\vec{v}_k(t)$ are calculated by the underlying physics engine based on the various forces that are acting on the joint and the segments they connect. This is the topic of the next section.

B. Dynamics

At any given time there are a number of forces that act on the body of the worm. These include gravity, friction, surface tension, inertia, elastic forces from the cuticle, force associated with internal pressure, dampening forces caused

Table II
PARAMETERS USED IN THE SIMULATION

Parameter	Description	Value	Units
L	Total length of the body	1000	μm
W	Total mass of the body	$5 \cdot 10^{-9}$	kg
S	Surface Tension	$2.0 \cdot 10^{4}$	G
F_m^{max}	Max muscle cell force	$6.5 \cdot 10^{-12}$	N
θ_m^{max}	Max muscle cell bend	$\frac{\pi}{10}$	rad
k_s	Torsional spring constant	$20 \cdot 10^{-12}$	$N \cdot m/rad$
k_p	Torsional pressure constant	$0.63 \cdot 10^{-12}$	$N \cdot m/rad$
b	Torsional damping constant	$0.2 \cdot 10^{-12}$	$N \cdot m \cdot s/rad$
μ_l	Coefficient of lateral friction	0.5	
μ_a	Coefficient of axial friction	5×10^{-3}	
λ_f	CPG wavelength	22	joints
Δt_f	CPG update interval	150	ms
λ_r	CPG wavelength	18	joints
Δt_r	CPG update interval	250	ms

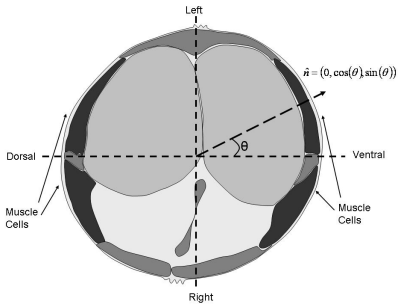

Figure 5. Cross-section showing the location of the muscle cells

by the incompressibility of liquid, and forces exerted by the muscles.

Fortunately, ODE handles gravitational, inertial, and frictional forces that act on the worm by allowing users to specify the mass (for computing gravitational and inertial forces) and the size, shape, and frictional coefficients for each of the segments of the body (for computing frictional forces). Tables I and II list the values that are used in our simulation.

Notable among these are the values for lateral and axial friction along with the value for surface tension. Currently, there are no exact values for the friction between the body of the worm and an agar surface. However, researcher believe that the alae that run the length of the worm's body act similar to an ice skate blade and creates very low axial friction while providing as much as 100 times the amount of lateral friction [2]. In our simulations, we have adopted an axial friction coefficient that is similar to a skate on ice, which is reported to be 0.005 [44] and use a value 100 time this amount for the lateral friction coefficient.

Unlike most organisms, the life of *C. elegans* is dominated by the force of surface tension, not gravity [45]. In fact, estimates for the surface tension experience by the worm are somewhere between 10,000 and 100,000 times the force of gravity [46]. At first, these numbers appear to be outrageously high, however we have recently conducted experiments using a high speed centrifuge, which, to our utter amazement, definitely show that the worms have no problem adhering to agar at forces of over 8,000 Gs. For our simulations, we chose to use a value of 20,000 Gs, which is simulated using a directional acceleration of $20000 \times -9.81 m/s^2$.

The forces that act on the joints are computed by our simulator about 100 times per second during each update of the physics model. The total force applied to a joint J_k at time t is calculated using the following equation:

$$\vec{F}_k^T(t) = \vec{F}_k^M(t) + \vec{F}_k^S(t) + \vec{F}_k^P(t) + \vec{F}_k^D(t) \qquad (3)$$

where $\vec{F}_k^M$ is the force exerted by the muscles, $\vec{F}_k^S$ is the force exerted by the elastic cuticle, $\vec{F}_k^P$ is the force exerted by the interior hydrostatic pressure, and $\vec{F}_k^D$ is a dampening force.

1) Muscle Forces: Muscle forces in *C. elegans* are produced by muscle cells that are attached to the cuticle of the body. These cells are arranged parallel to the anterior-posterior (AP) axis of the body in four rows with two rows on the dorsal and two rows on the ventral side. Figure 5 show a cross section of *C. elegans* showing the location of the muscles cells approximately half way down the AP axis. As can be seen in this figure, the muscle cells are offset by approximately 30 degrees left and right of the dorsal-ventral midline. Muscle cells are, therefore, named based on their AP position in the row and the row's position relative to the dorsal-ventral and left-right mid-lines. For example , the 7th muscle cell in the dorsal, right row is called MDR07. For simplicity, we refer to the set of muscle cells located at joint k as $m_k = \{MDL_k, MDR_k, MVL_k, MVR_k\}$.

For most of the worm's body, this offset has very little effect because the innervation pattern activates both the left and right muscle cells on a single side of the worm at the same time. This is not true in the head where a more complex innervation pattern allows the worm to lift its head

by activating the muscle on the left or right side at the same time.

We accounted for the offset placement of the muscle cells by calculating the force generated by each cell independently and multiplying that force by $\hat{\mathbf{n}}$, which is a unit vector normal to the surface of the worm. The normal vector is easily computed by $\hat{\mathbf{n}} = (\mathbf{0}, \pm\cos(\theta), \pm\sin(\theta))$ with signs being set appropriately according to quadrant location of the muscle cell. The following equation is used to calculate the muscle force applied to joint k at time t:

$$\vec{F}_k^M(t) = \sum_{m \in m_k} a_m \times F_m(\vec{\theta}_k(t)) * \hat{\mathbf{n}} \tag{4}$$

In the equation, a_m is the current activation level, a graded signal, of the muscle based on the inputs from the neurons innervating muscle cell m and $F_m(\vec{\theta}_k(t))$ is the maximum force that the cell can produce given its current length.

To compute $F_m(\vec{\theta}_k(t))$, we used a linear approximation to the Hill equation for the force/length relationship of muscle cells [47].

$$F_m(\vec{\theta}_k(t)) = (0.5k_s - \frac{F_m^{max}}{\theta_m^{max}}) \times |\vec{\theta}_k(t)| + F_m^{max} \tag{5}$$

Here, F_m^{max} is the maximum force that the cell produces at resting length, θ_m^{max} is the maximum angle that the joint can be displaced as a result of the contraction of the muscle and k_s is the spring constant associated with the elastic cuticle. The slope of this line is based on the spring constant of the cuticle such that these forces come to equilibrium when $|\vec{\theta}_k(t)| = \theta_m^{max}$ and both the right and left muscle are fully activated. This, by no means, limits the maximum bend angle of the joint. Both external and inertial forces can cause a joint to exceed θ_m^{max}. The values for these constants (Table II) were chosen based on values from [48] and [4] and were tuned using videos of worms during forward locomotion (see Section IV).

2) Spring, Pressure, and Damping forces: Whereas muscle force causes the body to deviate from it resting state, there are a number of forces that act to restore it. One of these forces is the elasticity of the cuticle, which can be modeled as a simple spring. Below is the equation for the force exerted by this spring:

$$\vec{F}_k^S(t) = -0.8 \times k_s \times \vec{\theta}_k(t) \tag{6}$$

The value for k_s is strongly related to the maximum muscle force and was chosen to be $k_s = 4 * F_m^{max}$. This creates a relationship between these values such that the average force applied over the range of dorsal or ventral muscle contraction is $\frac{1}{2}F_m^{max}$.

Along with the force created by the cuticle, internal pressure of the worm's body also exerts a restorative force. Recent measurements of the relationship between the elastic cuticle and the hydrostatic pressure using a piezoresistive displacement clamp have shown that the restorative force has a cuticle to pressure force ratio of 4 to 1 [49]. We used these finding to normalize the force associated with these two factors. Below is the equation we use for calculating the force associated with internal pressure:

$$\vec{F}_k^P(t) = -0.2 \times k_s \times \theta_m^{max} \tag{7}$$

We explicitly do not model the relationship between the change in volume and pressure as the body bends. We ignored this factor because it has been reported that total body volume does not change significantly over the worm's range of motion [2], [4]. This indicates that pressure acts a constant, not dynamic, restorative property, so we treat it as such.

Lastly, because of the structure and composition of the worm's body, it acts like a fluid-filled shock absorber. So, we apply a damping force to model the resistance that the body has to rapid changes in position using the formula below:

$$\vec{F}_k^D(t) = -b \times \vec{v}_k(t) \tag{8}$$

The value for b was derived through experimentation and is in line with value reported in [4].

Table III
SYNAPTIC WEIGHTS USED IN THE SIMULATION.

Forward				Reverse			
k	ω_k^f	**k**	ω_k^f	**k**	ω_k^r	**k**	ω_k^r
1	0.35	**13**	0.77	**1**	0.10	**13**	1.00
2	0.42	**14**	0.77	**2**	0.20	**14**	1.00
3	0.70	**15**	0.70	**3**	0.30	**15**	1.00
4	0.77	**16**	0.62	**4**	0.40	**16**	1.00
5	0.77	**17**	0.54	**5**	0.50	**17**	1.00
6	0.77	**18**	0.46	**6**	0.60	**18**	1.00
7	0.77	**19**	0.39	**7**	0.70	**19**	1.00
8	0.77	**20**	0.39	**8**	1.00	**20**	1.00
9	0.77	**21**	0.39	**9**	1.00	**15**	1.00
10	0.77	**22**	0.39	**10**	1.00	**22**	1.00
11	0.77	**23**	0.39	**11**	1.00	**23**	1.00
12	0.77	**24**	0.39	**12**	1.00	**24**	1.00

C. Locomotion Control

Because the major focus of this paper is on investigating a realistic physics model of *C. elegans*, we chose to implement a simple CPG for locomotion control similar to the one found in [2]. The CPG works by setting the activation level of the D-type interneuron that drives the B-type motor neurons during forward locomotion, and the A-type motor neurons during reverse locomotion. During forward locomotion this is done by setting the value in the first joint, $k = 1$ at each time t using the following formula:

$$a_{k=1}(t) = \sin(\frac{2\pi}{\lambda_f} \times t) \tag{9}$$

where λ_f is the wavelength for forward locomotion.

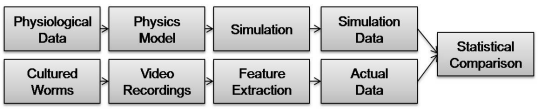

Figure 6. Methodology used to construct and validate the simulator.

At each successive time step $t + \Delta t_f$, the wave is propagated down the body such that for $2 \leq k \leq 24$

$$a_{k+1}(t + \Delta t_f) = a_k(t) \tag{10}$$

The value of Δt_f sets the characteristic frequency of the body wave for forward locomotion (see Table II). Initially, all of the activation levels are set to 0 and between subsequent updates the interneurons are held at their last activation level.

During reverse locomotion, the CPG sets the activation of the interneuron controlling the motor neurons in the last joint and propagates the wave from back to front. The wavelength and frequency of this wave is determined by the parameters Δt_r and λ_r.

The actual activation levels of the muscle cells a_m are dictated by three factors: (1) the activation level of the interneuron at the joint (a_k), (2) whether the worm is moving in forward or reverse, which determines if the A or B-type motor neuron is being activated by the interneuron, and (3) the synaptic strength of the connection between the motor neuron and the muscle cell ω_k^f or ω_k^r. The following equation shows this relationship during forward locomotion:

$$a_m = a_k \times \omega_k^f \tag{11}$$

In a close approximation to the cross inhibition circuit in *C. elegans*, when a_k is positive, the activation of the ventral muscles (MVL and MVR) are positive and the dorsal muscles (MDL and MDR) are 0. However, when a_k is negative, the activation of the dorsal muscles (MDL and MDR) becomes positive and the ventral muscles (MVL and MVR) are 0. The synaptic strength between the motor neurons and muscle cells were determined experimentally using data derived from video analysis of the worm in motion. Table III gives the weights that were found to produce a very close approximation to the gait of the worm during forward and reverse locomotion.

IV. Tuning and Validation

The value of a simulation can only be measured by cross-validating the data it produces against reality. In constructing and validating our simulation, we followed the process outline in Figure 6. The next phase of construction for the simulation was to tune and cross validate its performance against real worms. To do this, we used the *C. elegans* N2 wild type strain, which we obtained from the Caenorhabditis Genetics Center (CGC) at the University of Minnesota.

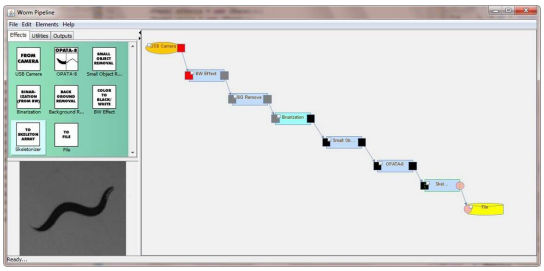

Figure 7. Screenshot of the WormAnalyzer

A. Materials and Methods

Maintenance and culturing of worms was performed as outlined in [50]. Worms were grown on standard NGM Lite plates with OP50 1CGJ *E. Coli* and incubated at $20°C$. The worms analyzed in these experiments were young adult worms (or, a mixture of young adult and adult worms), transferred while in L4 larval stage to freshly seeded OP50 plates the night before filming [51]. Worms were recorded on modified NGM Lite agar plates (3.0g KH2PO4, 0.5g K2HPO4, 2.0g NaCl, and Agar, without the addition of peptone or cholesterol) made specifically for the clarity of the recorded image. Worms were transferred to filming plates via a worm pick and filmed within thirty seconds of transfer, in order to take advantage of the higher locomotion activity exhibited by worms shortly after transfer. We found that this produced the most reliable and longest sustained locomotor activity.

Worms were filmed using a Leica S8 APO Stereomicroscope fitted with a ScopeTek MDC320 digital camera, outputting at a resolution of 1024x768 at 5 frames per second. The microscope was held at the 16x magnification setting during filming, with the illumination mirror angled to obtain images with the highest possible contrast. Individual worms were filmed for five minutes, during which the agar plate was moved manually, to re-position the worm within the microscope's field of view. A total of 487 minutes of raw video in 96 files was collected.

B. Image Processing

After collecting the video, we edited it to remove plate repositioning. Using consumer video editing software, we manually cut the raw footage and produced around 3.75 hours or 50,000 individual frames of forward locomotion and 21,000 frames or 2.33 hours of reverse locomotion.

To analyze this footage, we developed software, called the WormAnalyzer (see Figure 7, that is written in Java and based on the Java Media Framework (JMF). To do this, a set of JMF processors were constructed into a processing pipeline that converted each frame of the raw color video into a set of pixel locations that describes the position of the worms body. The WormAnalyzer software batch processes footage at about 5 times faster than real time. The analysis

pipeline we constructed is similar to that described in [51] with some minor improvements.

The first processor in the pipeline converts the video frames to grayscale and normalizes. This algorithm creates a histogram of color intensity for all pixels within a frame [52]. Using a threshold, we identify which intensities compose the majority of the image. This range of intensities is then converted to an easily identifiable solid color. This greatly diminishes the background noise that, if on the borders of a worm, can resist binarization and small object removal, ultimately skewing the thinning process.

Although the first step in the process converts the image to grayscale and removes most of the background, the second processor in the pipeline converts it to a binary image using a local thresholding algorithm. This algorithm uses a sliding 3 X 3 window to determine whether a given pixel should be converted to black (foreground) or white (background). This processor colors the pixel black if the standard deviation of the intensity of the pixel and its surrounding pixels is greater than the mean of the entire image, or if the mean intensity of the pixel and its surrounding pixels was greater than the background pixel intensity. Because the first processor converts the background to a solid color (white), this phase creates a very accurate binary image.

Next, we remove small objects from the image using a region labeling algorithm that indexes each pixel in the image according to the region that it belongs to. Once all of the black regions are labeled, we remove all of the regions except for the largest. This isolates the worm (colored black) onto a white background. We then used the same method to fill holes in the worms image by inverting the colors such that only the largest white region is maintained (the background).

The resulting binary image, now just the worm and the background, is passed through an implementation of the 8-distance, one-pass asymmetric thinning algorithm ($OPATA_8$) devised by Deng et al [53]. With noise resistance, better connectivity, and less erosion, the $OPATA_8$ implementation more quickly reduces the image to the core skeleton than the previously used triple pass thinning algorithm [54]. The resultant shape can have multiple endpoints but is ultimately trimmed down to a single representative skeleton by selecting the line connecting the two endpoints farthest from one another using the Floyd-Warshall algorithm [55].

The output of this process is a set of text files, which we refer to as body files. Each body file contains one line per frame of video with each line giving a timestamp and the pixel locations of the body of the worm. The number of pixels (or length of the body) is dependent on the size of the worm and also exhibits some variability due to the binarization of the image and subsequent thinning.

Because we wanted to gather statistics based on a nonuniform segmentation of the worms body, it was necessary to identify the location of the worms head. To aid in this process, software was developed to show the first frame of each video file in a directory. To indicate the location of the head, a researcher simply clicked on the head end of the worm. A head tag was then inserted into the corresponding body file that identified the location of the head in the first frame. With the head tag in place, subsequent frames of the video were properly rearranged such that the end point closest to the last head location was identified as the head. This turns out to be a very robust and reliable mechanism if the video being processed was taken at high enough frame rates.

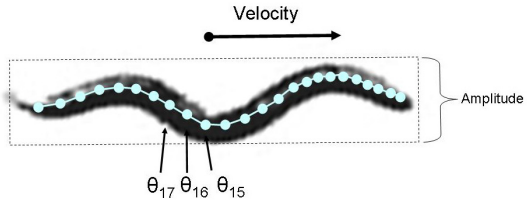

Figure 8. Features of *C. elegans* locomotion

These head-tagged body files are then post-processed in batches. The software takes a directory of head-tagged body files and produces skeleton files that provide a description of the location and position of each segment of the worm. Like the simulator, the size of these segments are not uniform, but are based on the muscle placement as reported in [43]. For convenience, the simulator also creates skeleton files in exactly the same format as the WormAnalyzer. This allows us to directly compare the output from both processes using the same metrics calculated in exactly the same way.

The skeleton files are then processed to extract features of the worms movement using a technique similar to the one reported in [23]. Currently, this software extracts 49 features from the worms motion including the velocity of the centroid of the worm, the amplitude of the worms body, the average angle at each joint location, and the angular to simulated results velocity of each joint (see Figure 8). The software outputs data files that give these features on a frame by frame basis and a set of summary statistics that can be further analyzed using statistical packages.

C. Simulator Data Collection

To collect data from the simulator, the physics model of the worm was instrumented to output the position of each of the joints five times a second to a skeleton file. The CPG was first set to generate forward locomotion and 20 minute long data runs were performed. At the end of each run, the simulator was restarted. We then repeated the experiment while running the CPG in reverse. In total 48,000 data points of both forward and backward locomotion were collected, accounting for approximately 5 hours of runtime. We then processed the skeleton files using the WormAnalyzer.

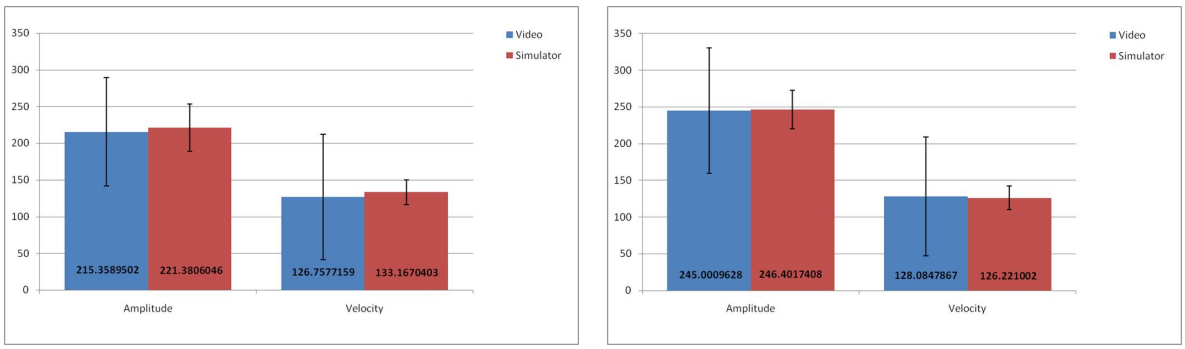

(a) Forward (b) Reverse

Figure 9. Comparison of locomotion velocity and amplitude of *C. elegans* to simulated results

V. Discussion

Figures 9, 10, and 11 present the results of both the analysis of the video and the simulator. The results for the video are similar with the results obtained in both [3] and [23]. Essentially, it can be seen that the amplitude of the body during forward locomotion is about 21.5% of the length of the body and the instantaneous centroid velocity is about 126 $\mu m/sec$. For reverse locomotion we obtained an average amplitude of 24.5% of the length of the body and a centroid velocity of 128 $\mu m/sec$. These number are similar to the values reported in [23], which gives a forward centroid velocity of 180 ± 30 $\mu m/sec$ and an amplitude of $19.27 \pm 2.34\%$. We believe the discrepancy in velocity is a result of the worms occasionally pausing during our video recordings. We found that obtaining such a slow velocity was very difficult in the simulations.

Figures 10 and 11 show that as the wave propagates down the body that its amplitude decreases as is evident by the bend angles that are produced in these regions. This is similar to the shape of the average flex angles that are reported in [3]. However, we noticed that in our video results, the bend angles increase near the tail of the worm as opposed to continuing to decrease as was reported in [3].

When comparing the video results to the simulated results we see that, with the exception of the angles at the head and tail of the worm, our simulator accurately reproduces the velocity, amplitude, individual angles, and angular velocities of the real worm. We have analyzed the reason for the discrepancy at the head and tail and have concluded that it is caused by data that is not being collected at high enough resolution. The simulation uses a worm of 100 units long with each unit representing $10\mu m$. This makes the second segment of the worm exactly 1 unit in length. When using integers to represent the location of the joints connected to this segment to calculate the angles, it allows only values that are multiples of $45°$. The same error is probably being introduced in the video analysis, but is stabilized by the variability of the worm's length. Overall, these factors effect the analysis, but not the actual behavior of the simulated worm, which by all appearances precisely reproduces the motion of the real organism.

Analytically, the frequency of the CPG used to drive forward locomotion is about 0.3Hz. Even though this is within one standard deviation of the value of 0.36 ± 0.08 Hz for N2 wild type reported in [23], it is still slightly below the expected value. This is entirely expected as the velocity that we produce is lower and the amplitude slightly higher than was reported in that work. We are very confident that changing the values of either λ_f or Δt_f will cause our simulation to reproduce the values they report.

To drive reverse locomotion, the frequency of the CPG is about 0.22Hz. This value is less than the one used for forward locomotion, but a lower frequency was also reported in [3] for reverse locomotion.

We would also like to mention that the process of tuning a CPG to produce the gait of the worm was a very difficult endeavor. There were two issues that we encountered that complicated the task. First, if the weight of the synapse between the interneurons and the motor neurons are uniform, then the model has a tendency to tail whip during forward locomotion. This is caused by a decrease in the wavelength of the wave as it propagates down the body when the worm is in motion, which causes high inertial forces to be exerted. On further investigation we found references to this decrease in wavelength in living worms [22], [30]. To compensate for this effect, we decreased the weight associated with muscles in the rear of the worm, which not only removed the tail whip, but normalized the bend angles to match those observed in the video analysis.

We believe that this indicates that during forward locomotion the worm generates most of its propulsive forces using the muscles located in the anterior. The posterior portions of the worm are likely to apply just enough force to maintain the wave and prevent a loss of energy due to drag. The physiological layout of the worm's musculature seems to support this claim as about 63% of the muscles lie

anterior of the AP midline. We also believe that this has not been observed in other simulations because of the uniform representation of individual segments of the body, the lack of torsional inertial force, and the lack of explicit modeling of the friction caused by variations in surface contact.

The second issue we encountered was the difference in muscle force needed for forward and reverse locomotion. When we first attempted reverse locomotion, we simply reversed the wave pattern. We quickly noticed that the worm was unable to move because the lower concentration of muscles near the tail could not produce enough force. By increasing the maximum muscle force, we were able to get the worm to move in reverse, but then needed to scale back the synaptic weights used during forward locomotion. This could indicate two things. First, it may that the muscles don't need to be flexed with full force during forward locomotion because of their placement. The smaller amplitude and increased frequency used during forward locomotion seem to support this conjecture. It may also indicate that the actual worm does not generate more force while reversing, but is generating it in a different way, driving the movement using the anterior muscles. A more detailed analysis of dynamics of reverse locomotion is needed in order to determine if one or both of these hypotheses is true.

VI. Conclusion

In this paper we presented a new, biologically accurate, three dimensional model of the body of the nematode *Caenorhabditis elegans*. We tuned and validated this model against values derived from both current literature and from analysis of video recordings taken of the worm during forward and reverse locomotion. In the process of performing the tuning, we discovered two new insights into the mechanisms of locomotion employed by *C. elegans*. First, our model shows that worms may derive most of their forward propulsive force from the muscles in the anterior portion of their body with the posterior portions just propagating the wave in an energy minimizing way. Second, we found that in order to perform reverse locomotion that the muscles needed to generate 23% more force than used while moving forward. This may indicate that moving forward actually requires less force from each of the muscles or that reverse locomotion is also predominantly driven using its anterior muscles.

Acknowledgment

The authors would like to thank the CGC for providing the N2 strains used in this paper, Melanie Smith for insightful discussions, Mike Michalek for his assistance in editing the video files, Jason Avery for culturing and videotaping the worms, and the members of the Rand Lab at the Oklahoma Medical Research Foundation (OMRF) for providing their protocols and support on numerous occasions.

The authors gratefully acknowledge support of the Defense Advanced Research Projects Agency under DARPA grants HR0011-07-C-0060. Views and conclusions contained in this document are those of the authors and do not necessarily represent the official opinion or policies, either expressed or implied of the US government or of DARPA.

References

[1] R. Mailler, J. Avery, J. Graves, and N. Willy, "A biologically accurate 3d model of the locomotion of caenorhabditis elegans," in *Proceedings of First International Conference on Computational and Systems Biology and Microbiology (BIOSYSCOM)*, 2010.

[2] E. Neibur and P. Erdös, "Theory of the locomotion of nematodes: Dynamics of undulatory progression on a surface," *Biophysics Journal*, vol. 60, pp. 1132–1146, November 1991.

[3] J. Karbowski, G. Schindelman, C. Cronin, A. Seah, and P. Sternberg, "Systems level circuit model of c. elegans undulatory locomotion: mathematical modeling and molecular genetics," *Journal of Computational Neuroscience*, vol. 24, pp. 253–276, 2008.

[4] M. Wakabayashi, "Computational plausibility of stretch recpetors as the basis for motor control in c. elegans," Master's thesis, University of Queensland, 2006.

[5] J. Bryden and N. Cohen, "Neural control of caenorhabditis elegans forward locomotion: the role of sensory feedback," *Biological Cybernetics*, vol. 98, pp. 339–351, 2008.

[6] W. B. Wood, *The Nematode Caenorhabditis elegans*. Cold Springs Harbor Laboratory Press, 1988, ch. Introduction to C. elegans Biology.

[7] M. Driscoll and J. Kaplan, *C. elegans II*. Cold Spring Harbor Laboratory Press, 1997, ch. Mechanotransduction.

[8] J. Rand and M. Nonet, *C. elegans II*. Cold Spring Harbor Laboratory Press, 1997, ch. Synaptic Transmission.

[9] J. White, E. Southgate, J. Thomson, and S. Brenner, "The structure of the nervous system of the nematode caenorhabditis elegans," in *Royal Society of London Philosophical Transactions*, ser. Series B, vol. 314, 1986, pp. 1–340.

[10] J. Richmond and E. Jorgensen, "One gaba and two acetylcholine receptors function at the c. elegans neuromuscular junction," *Nature Neuroscience*, vol. 2, pp. 791–797, 1999.

[11] J. Sulston, M. Dew, and S. Brenner, "Dopaminergic neurons in the nematode caenorhabditis elegans," *Journal of Comparative Neurology*, vol. 163, pp. 215–226, 1975.

[12] R. Lints and S. Emmons, "Patterning of dopaminergic neurotransmitter indentity among caenorhabditis elegans ray sensory neurons by a tgfβ family signaling pathway and a hox gene," *Development*, vol. 126, pp. 5819–5831, 1999.

[13] S. Srinivasan, L. Sadegh, I. Elle, A. Christensen, N. J. Faergeman, and K. Ashrafi, "Serotonin regulates c. elegans fat and feeding through independent molecular mechanisms," *Cell Metabolism*, vol. 7, pp. 533–544, 2008.

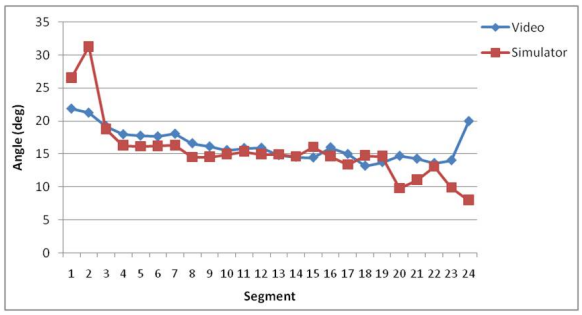

(a) Forward

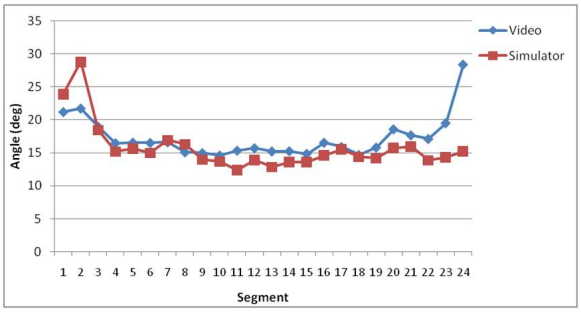

(b) Reverse

Figure 10. Comparison of bend angles in *C. elegans* to simulated results

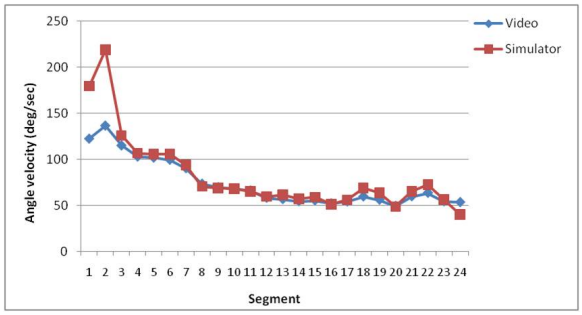

(a) Forward

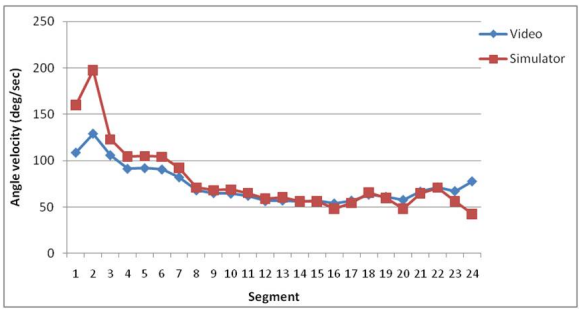

(b) Reverse

Figure 11. Comparison of bend velocities in *C. elegans* to simulated results

[14] C. Trent, N. Tsung, and H. Horvitz, "Egg-laying defective mutants of the nematode caenorhabditis elegans," *Genetics*, vol. 104, pp. 619–647, 1983.

[15] A. Hart, S. Sims, and J. Kaplan, "Synaptic code for sensory modalities revealed by c. elegans glr-1 glutamate receptor," *Nature*, vol. 378, pp. 82–85, 1995.

[16] M. Goodman, D. Hall, L. Avery, and S. R. Lockery, "Active currents regulate sensitivity and dynamic range in c. elegans neurons," *Neuron*, vol. 20, pp. 763–772, 1998.

[17] C. Bargmann and L. Avery, "Laser killing of cells in caenorhabditis elegans," *Methods in Cell Biology*, vol. 48, pp. 225–249, 1995.

[18] L. Avery and H. Horvitz, "Pharyngeal pumping continues after laser killing of pharyngeal nervous system of c. elegans," *Neuron*, vol. 3, pp. 473–485, 1989.

[19] E. Tsalik and O. Hobert, "Functional mapping of neurons that control locomotion behavior in caenorhabditis elegans," *Journal of Neurobiology*, vol. 56, no. 2, pp. 178–197, 2003.

[20] J. Gray, J. Hill, and C. Bargmann, "A circuit for navigation in caenorhabditis elegans," *Proceedings of the National Academy of Sciences USA*, vol. 102, pp. 3184–3191, 2005.

[21] S. McIntire, E. Jorgensen, and H. Horvitz, "The gabaergic nervous system of caenorhabditis elegans," *Nature*, vol. 364, pp. 334–337, 1993.

[22] J. Korta, D. A. Clark, C. V. Gabel, L. Mahadevan, and A. D. T. Samuel, "Mechanosensation and mechanical load modulate the locomotory gait of swimming c. elegans," *Journal of Experimental Biology*, vol. 210, p. 23832389, 2007.

[23] C. J. Cronin, J. E. Mendel, S. Mukhtar, Y.-M. Kim, R. C. Stirbl, J. Bruck, and P. W. Sternberg, "An automated system for measuring parameters of nematode sinusoidal movement," *BMC Genetics*, vol. 6, no. 5, February 2005.

[24] C. Bargmann and I. Mori, *C. elegans II*. Cold Spring Harbor Laboratory Press, 1997, ch. Chemotaxis and Thermotaxis.

[25] M. Driscoll and J. Kaplan, *C. Elegans II*. Cold Springs Harbor Laboratory Press, 1997, ch. Mechanotransduction.

[26] A. Stretton, R. David, J. Angstadt, J. Donmoyer, and C. Johnson, "Neural control of behavior in ascaris," *Trends in Neuroscience*, vol. 8, pp. 294–300, 1985.

[27] E. Neibur and P. Erdös, "Theory of locomotion of nematodes: Control of the somatic motor neurons by interneurons," *Mathematical Biosciences*, vol. 118, no. 1, pp. 51–82, 1993.

[28] J. Bryden, "A simulation model of the locomotion controllers for the nematode caenorhabditis elegans," Master's thesis, University of Leeds, 2004.

[29] J. H. Boyle and N. Cohen, "Caenorhabditis elegans body wall muscles are simple actuators," *Biosystems*, vol. 94, pp. 170–181, 2008.

[30] S. Berri, J. H. Boyle, M. Tassieri, I. A. Hope, and N. Cohen, "Forward locomotion of the nematode c. elegans is achieved through the modulation of a single gait," *HSFP Journal*, vol. 3, no. 3, pp. 186–193, 2009.

[31] M. Suzuki, T. Tsuji, and H. Ohtake, "A dynamic body model of the nematode c. elegans with touch-response circuit," in *Proceedings of the 2005 IEEE International Conference on Robotics and Biomimetics*, 2005, pp. 538–543.

[32] M. Rönkkö and G. Wong, "Modeling the c. elenags nematode and its environment using a particle system," *Journal of Theoretical Biology*, vol. 253, pp. 316–322, 2008.

[33] T. Ferree, B. Marcotte, and S. Lockery, "Neural network models of chemotaxis in the nematode caenorhabditis elegans," in *Advances in Neural Information Processing Systems*, M. Mozer, M. Jordan, and T. Petsche, Eds. MIT Press, 1997, pp. 55–61.

[34] T. Ferree and S. Lockery, *Computational Neuroscience: Trends in Research*. Plenum Press, 1998, ch. Chemotaxis Control by Linear Recurrent Networks.

[35] S. Wicks, , C. Roehrig, and C. Rankin, "A dynamic network simulation of the nematode tap withdrawal circuit: Predications concerning synaptic function using behavioral criteria," *The Journal of Neuroscience*, vol. 16, no. 12, pp. 4017–4031, 1996.

[36] M. Powell, "Java monkey engine v2.0." [Online]. Available: http://www.jmonkeyengine.com

[37] R. Smith, "Open dynamics engine." [Online]. Available: http://www.ode.org

[38] O. S. Project, "Java monkey engine physics v2.0." [Online]. Available: https://jmephysics.dev.java.net/

[39] D. Baraff, "Fast contact force computation for nonpenetrating rigid bodies," in *Proceedings of SIGGRAPH 94*, July 1994, pp. 23–34.

[40] O. S. Project, "Gazebo." [Online]. Available: http://playerstage.sourceforge.net/index.php?src=gazebo

[41] AnyKode, "Marilou." [Online]. Available: http://www.anykode.com

[42] Cyberbotics, "Webots v6." [Online]. Available: http://www.cyberbotics.com/

[43] L. R. Varshney, B. L. Chen, E. Paniagua, D. H. Hall, and D. B. Chklovskii, "Structural properties of the caenorhabditis elegans neuronal network," 2009. [Online]. Available: http://www.citebase.org/abstract?id=oai:arXiv.org:0907.2373

[44] J. de Koning, G. de Groot, and G. J. van Ingen Schenau, "Ice friction during speed skating," *Journal of Biomechanics*, vol. 25, no. 6, pp. 565–571, 1992.

[45] D. L. Riddle, T. Blumenthal, B. J. Meyer, and J. R. Priess, *C. elegans II*. Cold Spring Harbor Laboratory Press, 1997, ch. Introduction to C. elegans.

[46] N. Szewczyk, *Basic Biology for Engineers*. NASA Ames, 2003, ch. Unit 4.2: C. elegans Biology.

[47] A. V. Hill, "The heat of shortening and the dynamic constants of muscle," in *Proceedings of the Royal Society of London*, ser. B, vol. 126, 1938, pp. 136–195.

[48] J. H. Boyle, J. Bryden, and N. Cohen, "An integrated neuromechanical model of c. elegans forward locomotion," in *Neural Information Processing: 14th International Conference, ICONIP 2007*. Berlin, Heidelberg: Springer-Verlag, 2008, pp. 37–47.

[49] S.-J. Park, M. B. Goodman, and B. L. Pruitt, "Analysis of nematode mechanics by piezoresistive displacement clamp," in *Proceedings of the National Academy of Sciences*, vol. 104, no. 44, 2007, pp. 17 376–17 381.

[50] S. Brenner, "The genetics of caenorhabditis elegans," *Genetics*, vol. 77, pp. 71–94, 1974.

[51] W. Geng, P. Cosman, C. C. Berry, Z. Feng, and W. R. Schafer, "Automatic tracking, feature extraction and classification of c. elegans phenotypes," *IEEE Transactions on Biomedical Engineering*, vol. 51, no. 10, pp. 1811–1820, October 2004.

[52] M. Nixon and A. Aguado, *Feature Extraction and Image Processin*, 2nd ed. Academic Press, 2008.

[53] W. Deng, S. S. Iyengar, and N. E. Brener, "A fast parallel thinning algorithm for the binary image skeltonization," *The International Journal of High Performance Computing Applications*, vol. 14, no. 1, pp. 65–81, 2000.

[54] T. Zhang and C. Y. Suen, "A fast parallel algorithm for thinning digital patterns," *Communications of the ACM*, vol. 27, no. 3, pp. 236–239, March 1984.

[55] T. H. Cormen, C. E. Leiserson, R. L. Rivest, and C. Stein, *Introduction to Algorithms (3rd ed.)*. MIT Press., 2009, ch. Chapter 25: All-Pairs Shortest Paths.